35th Annual International Conference of the IEEE EMBS
Osaka, Japan, 3 - 7 July, 2013

Microwave Breast Tumor Detection and Size Estimation Using Contrast-Agent-Loaded Magnetotactic Bacteria

Yifan Chen[1], Panagiotis Kosmas[2], and Sylvain Martel[3]

Abstract— **We propose a new approach to microwave breast tumor detection based on the use of bio-compatible flagellated magnetotactic bacteria (MTB). Previous work has shown that the directions and speeds of these bacterial microrobots adapted to operate in human microvasculature can be guided along pre-planned paths deep inside the human body through external magnetic fields. Furthermore, a microwave contrast agent can be loaded onto MTB to alter the dielectric properties of tissues near the agent. Based on these two phenomena, we illustrate how multiple agglomerations of MTB released into human breast could be tracked simultaneously and monitored using differential microwave imaging (DMI) techniques. We also present novel strategies to detect and localize a breast cancerous mass as well as estimate its size through this new DMI-trackable bacterial propulsion and steering approach, and use an anatomically realistic breast model as a testbed to verify the feasibility of this breast cancer diagnostic technique.**

I. Introduction

In recent years, there have been considerable efforts in applying microwave technology for early stage breast cancer detection [1]. However, the efficacy of microwave medical imaging can be affected by strong interference due to normal tissue heterogeneities. Similar to other imaging modalities, the use of a contrast medium such as carbon nanotubes (CNTs) or magnetic nanoparticles (MNPs) can potentially alter the dielectric properties of the tumor and enable detection [2], [3]. Unfortunately, current targeting techniques often suffer from limited efficacy due to intratumoral penetration limitations and the presence of quiescent cells within tumors [4]. As a result, only a low volumetric concentration of contrast agent is able to reach cancer cells.

Bio-compatible flagellated magnetotactic bacteria (MTB) with nanometer-sized magnetosomes acting like computer-controlled medical microrobots have been suggested as efficient carriers for tumor targeting applications [5]. The MTB directions and displacement speeds can be controlled by an external magnetic field to transport efficiently a nanoload such as contrast agent to a tumor location in deep regions of the human body. A strategy for MTB-assisted microwave breast tumor sensing and targeting was proposed in [6], where each time a single swarm of MTB loaded with a nanocomposite contrast agent is injected into human breast from a pre-defined infusion site. The MTB will align in the direction of an external magnetic field and its motion could potentially be tracked by using the differential microwave imaging (DMI) technique proposed in [7], [8]. In theory, when a particular swarm trajectory would meet a tumor, the contrast agent will be unloaded and bound to cancer cell receptors. The site where the contrast agent eventually accumulates will correspond to an MTB footprint "sink" inside breast.

The current work extends the results in [7], [8] by considering multiple agglomerations of MTB, which are administered simultaneously into the breast at each round of injection to reduce the sensing time. Furthermore, we demonstrate how we can deploy the MTB agglomerations to target possible tumor locations from different angles in order to reduce false alarms and estimate the tumor size *via* registration of multiple final footprints around the tumor border.

The remainder of the paper is organized as follows. In Section II, we highlight some key properties of controllable MTB actuators, which have been experimentally demonstrated by Martel *et al.* [5]. In Section III, we describe possible schemes to detect and localize breast tissue malignancy as well as estimate its size through the DMI-trackable bacterial propulsion and steering platform. In Section IV, we study the feasibility of the proposed solution using an anatomically realistic breast model from the University of Wisconsin Computational Electromagnetics (UWCEM) Laboratory's breast phantom repository [9], and we conclude with some additional remarks in Section V.

II. Main Characteristics of MTB

Flagellated MTB include the following components as illustrated in Fig. 1(a): (i) a chain of magnetosomes imparting to the MTB a magnetic moment so that the bacterium can align itself to an external magnetic field; (ii) two flagellar bundles allowing the bacterium to swim in a medium; (iii) a fuel unit powering all the components by scavenging energy from external sources; and (iv) sensors acting as the interface between the environment and the MTB . As shown in the previous works by Martel *et al.* (see e.g., [5]), MTB exhibit the following desirable properties making them ideal controllable bacterial actuators for direct tumor sensing.

Speed and size: Magnetotactic cocci cells (e.g., the MC-1 bacteria) can achieve an average velocity of 200 μm/s in human blood with a peak velocity of 300 μm/s. The maximum velocity is not significantly affected when the MTB were loaded with an average of 70 liposomes with an

[1]Y. Chen is with the Department of Electronic Engineering, South University of Science and Technology of China, Shenzhen, China 518055, chen.yf@sustc.edu.cn.

[2]P. Kosmas is with the School of Natural and Mathematical Sciences, King's College London, London, U.K., WC2R 2LS, panagiotis.kosmas@kcl.ac.uk.

[3]S. Martel is with the Department of Computer Engineering, Ecole Polytechnique de Montreal, Montreal, Canada H3T 1J4, sylvain.martel@polymtl.ca.

978-1-4577-0216-7/13/$26.00 ©2013 IEEE

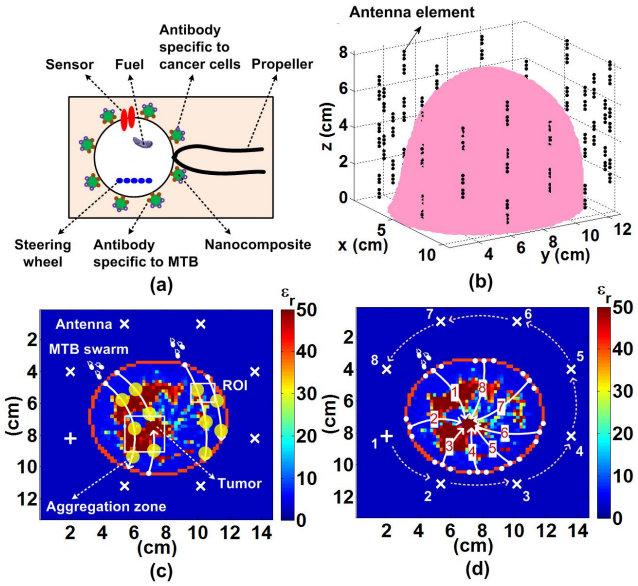

Fig. 1. (a) Key functional elements of an MTB. (b) Illustration of the tumor sensing and diagnosis system using a configuration similar to [7]. (c) Dielectric profile at 1 GHz for the coronal cross-section through the third antenna ring. We assume concentric magnetic field lines originating from a dc source via one of the antennas (marked with a '+') during the propulsion-and-steering phase. All the eight antennas probe the breast sequentially with UWB pulses during the tracking phase after the MTB reach the targeted aggregation zones (marked with yellow circles). Two clumps of MTB are released simultaneously into the breast. (d) Size estimation of the tumor by targeting it from different angles; the eight antennas are sequentially employed to carry a dc for generation of magnetic fields.

overall diameter exceeding 150 nm suggesting the possibility of attaching a wide variety of nanoscale elements to the surface of its cell. The cell of the MC-1 MTB is spherical in shape with a diameter of ~ 2 μm being approximately half the diameter of the smallest capillaries in human, making it ideal for transiting in the tiniest blood vessels.

Propulsion and steering: The two flagellar bundles of the MC-1 MTB provide a thrust force exceeding 4 pN, which is much higher than most other flagellated bacteria ($0.3-0.5$ pN). When subject to a magnetic field higher than approximately 4 Gauss, the directional motions of the MTB were mainly influenced by magnetotaxis (i.e., aligned to magnetic field lines) as compared to chemotaxis (i.e., moving towards or away from a chemical source) and aerotaxis (i.e., moving towards or away from air or oxygen), thus fully controllable by electronics and computer.

Bio-compatibility and lifespan: The degradation products of the nonpathogenic bacteria could have a cytotoxic effect at high concentration. Preliminary results showed that the cell viability was higher than 90% for 80 μl of bacteria solution (5×10^4 cells/200 μl in cell culture solution) in a 200 μl well, indicating the noncytotoxic effect of the bacteria at this volume. On the other hand, initial experiments conducted in human blood at 37° showed that the velocity V (in μm/s) at a time t (expressed in minute) after the beginning of operations of the MC-1 MTB decreased according to

$$V = 0.09t^2 - 8.10t + V_0, \quad 0 \le t \le 40 \text{ min} \qquad (1)$$

where $V_0 \approx 200$ μm/s is the initial average velocity of the MTB prior to being injected into blood. The MC-1 MTB would remain effective for at least 40 minutes, and the decrease in speed was probably caused by the relatively high temperature of blood. This is beneficial from the perspective of bio-compatibility and safe *in vivo* operations, but limits the time at which the MC-1 MTB could operate. As a ballpark figure, the average distance that could be traveled by an effective MC-1 MTB in human body is given by $\int_0^{40} V \cdot 60 \mathrm{d}t \approx 21$ cm, which is sufficient for the application of breast cancer theranostics.

Loading and targeting: The delivery of a contrast agent to a tumoral lesion requires transitions through capillary sections of human microvasculature. The loading strategy depicted in Fig. 1(a) can utilize antibodies specific to MC-1 cells or another effective method based on chemical bounding (see e.g., [5]). The nanocomposites such as CNTs can be functionalized by means of proper molecular groups such as peptides or antibodies, which are able to bind to cancerous cell receptors. In order to deliver sufficient amount of contrast agent to a tumor, a cluster of MC-1 MTB could be deployed simultaneously. It has been demonstrated that an agglomeration of MC-1 cells could be controlled like an unified organism to swim along a pre-determined path by an external computer [10]. Finally, it has been shown using an *in vitro* model that MTB guided by magnetic fields could penetrate inside a multicellular tumor spheroid. As many tumors contain vasculogenic mimicry, these channels should help MTB to be evenly distributed inside a tumor.

Aggregation of MTB: A relatively weak magnetic gradient could be generated towards an *aggregation zone*, whose size can easily be in the millimeter range. The boundary of the aggregation zone is equivalent to approximately 0.5 Gauss with the center at 0 Gauss. When outside the aggregation zone, the bacteria follow the line of magnetic field. When inside the zone, the MTB is no longer influenced by magnetotaxis and begin random motions. If the MTB exit the aggregation zone, the magnetic field forces the MTB to move back to the zone by magnetotaxis. To improve targeting effectiveness, various magnetic field modulation modes have been developed depending on the characteristics of the angiogenesis network, i.e., the capillary network feeding the tumor, or the surrounding tissue. Once targeting has been completed, imaging could be performed to assess targeting efficacy and to confirm the region being affected. If needed, the operation can be repeated towards another targeted area by setting the aggregation zone accordingly.

III. Strategies for Breast Tumor Detection, Localization, and Size Estimation

In this section we summarize our proposed strategy, which has improved upon the original method presented in [6], [8], and elaborate on the additional multi-directional targeting approach. Our simulations are based on the same "heterogeneously dense" breast phantom from the UWCEM repository [9], and the same assumptions as in [6]–[8], which are summarized in Fig. 1(a)-(c). The multi-directional targeting

approach is illustrated in Fig. 1(d). The basic sequence of events is detailed as follows.

Initialization: Prior to the injection procedure, we sequentially transmit ultra-wideband (UWB) radar pulses from each antenna element to probe the breast as shown in Fig. 1(c), and record the backscatter response at each element. These data in the absence of contrast agent will be used as the benchmark information in the DMI operation at a later stage.

Propulsion and steering: We plan the MTB paths in the breast based on its geometry as well as the regions-of-interest (ROIs) in its interior, and determine the injection sites on the breast surface. This survey plan should ensure that the entire ROIs is covered. To reduce sensing time, we infuse multiple clusters of contrast-agent-attached MTB into the breast. We assume that the swarms are guided along concentric magnetic fields generated at one of the eight antennas for a specific interval $t_{\rm PS}$ until they reach the targeted aggregation zones as illustrated in Fig. 1(c). During traveling to the aggregation zone, the MTB are not detected because they swim at different velocities and as such they disperse, making the density too low for tracking.

Tracking: Subsequently, we switch the system setting from the propulsion-and-steering mode to the tracking mode. In order to set two aggregation zones simultaneously, we employ the following time-multiplexing scheme at a high frequency: $T_{\mathcal{M}_1} \rightarrow T_{\mathcal{M}_2} \rightarrow T_{\mathcal{A}_1} \rightarrow T_{\mathcal{M}_1} \rightarrow T_{\mathcal{M}_2} \rightarrow T_{\mathcal{A}_2} \rightarrow \cdots$. During $T_{\mathcal{M}_1}$ and $T_{\mathcal{M}_2}$, two magnetic gradients are generated to set the two aggregation zones. Furthermore, during $T_{\mathcal{A}_i}$ $(i = 1, 2, \cdots, 8)$, the waveform used in the initialization phase is re-transmitted from the ith antenna element, and the corresponding backscatter response is recorded. We then apply the DMI algorithm to track multiple swarms within their respective aggregation zones. The size of the aggregation zones is in the range of less than 2 mm, which is much smaller than the cancerous lesion to be detected.

Decision-making: We then decide whether the tumor sensing process is complete, given the MTB tracks and subject to the criteria given in [8]. If an agglomeration of bacteria fail to sense a tumor (i.e., the corresponding MTB path does not intersect the tumor), it will keep navigating in capillary channels in the directions aligned to the magnetic field lines until being guided out of human body. On the other hand, if the swarm detects a tumor, the contrast medium will be unloaded and bound to cancer cell receptors. Once unloaded, this swarm will no longer be visible by DMI, which only tracks differences in tissue microwave properties due to the agent. Thus, the site where the contrast agent eventually accumulates will correspond to a "sink" of the observable aggregation zones along the pre-planned MTB trajectory. In order to ensure successful detection and targeting of multiple cancerous masses, all pre-planned MTB trajectories should be completed even if a tumor has been detected.

Multi-directional targeting: Provided with the *a priori* knowledge of the tumor location acquired in the previous steps, we then re-plan the MTB paths and injection sites in order to target the tumor from many different angles. The survey plan should ensure that these angles-of-arrival are evenly distributed between 0 and 2π to facilitate a full 360-degree view of the tumor. A possible strategy is shown in Fig. 1(d), where each antenna (indexed from 1 to 8) takes turn to carry a dc for generation of magnetic fields. Suppose that we have extracted the rough position of a tumor through the previous operations. For each dc excitation, we can identify a few adjacent infusion sites on the breast surface as shown in Fig. 1(d). These sites are selected such that theoretical MTB paths originated from them may intersect at the tumor. For illustrative purposes, we draw one path (marked with the antenna index) for each antenna as depicted in Fig. 1(d). We then administer MTB and perform propulsion, steering, and tracking until all the "sinks" are observed. If the distance between two successive footsteps is sufficiently small, the final footprints of MTB provide markers on the tumor edge and therefore, can be used to approximate its size. This additional step also helps reduce false alarms for tumor detection and localization by exploiting MTB path diversity.

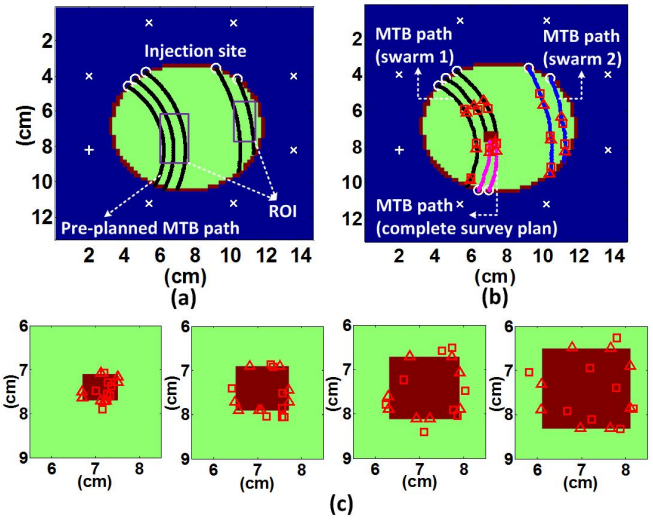

Fig. 2. (a) Pre-planned MTB paths for the system setup in Fig. 1(c). (b) Simulated DMI footprints. The MTB injection sites are marked with "○". The actual and estimated positions of the MTB in the aggregation zones during the tracking phase are marked with "△" and "□", respectively. The estimated final destination of contrast agent (i.e., DMI footprint "sink") is marked with "★". (c) Simulated DMI footprints for four tumors with different sizes. The actual and estimated final MTB footprints are marked with "△" and "□", respectively.

IV. Simulation Results

In order to elaborate on the tumor sensing and diagnosis strategies highlighted above, we have simulated possible motions of the swarms due to the assumed magnetic field and test the DMI's ability to track their trajectories and detect the tumor. The injection sites are spaced on the surface of the 2-D cross-sectional plane of the phantom depicted in Fig. 1(c), which is also illustrated in Fig. 2(a) (marked with circles). Fig. 2(a) also illustrates the pre-planned MTB routes covering uniformly the two ROIs in the breast interior; the distance between two adjacent paths is around 5 mm. Two

MTB agglomerations are released into the breast at the same time, and their infusion sites are spaced apart during the entire sensing process.

We assume that each population of MTB follows a directional random walk during the propulsion-and-steering stage. Consequently, each step size of swarm varies according to an exponential distribution with a mean value β, and the direction at each step is uniformly distributed between $[\varphi - \theta, \varphi + \theta]$. Here φ is the mean direction aligned with the tangent of the magnetic field and θ measures the impact of random directional disturbance caused by other gradients (chemotaxis and aerotaxis) and irregular microvasculature networks. The existing experimental results suggest that θ is usually quite small. Finally, we assume that the MTB in the aggregation zones follow an isotropic random walk with the same step size distribution during the tracking stage, as demonstrated experimentally. The initial speeds of both swarms prior to injection are chosen as $200\ \mu\mathrm{m/s}$, and decrease with time in the breast according to (1). The duration for the propulsion-and-steering phase is $t_{\mathrm{PS}} = 2\ \mathrm{min}$. To simulate the impact of agent-loaded MTB on the dielectric properties of breast tissues, we consider that they induce changes in the tissue dielectric properties for a volume represented by a $2 \times 2 \times 2\ \mathrm{mm}^3$ cubic voxel inside the breast phantom. We assume the relative permittivity and conductivity of this voxel to be 22% and 70% higher than the median properties of malignant glandular breast tissue, inspired by results for CNTs in [2].

A typical simulated sensing process ($\theta = 30°, \beta = 100\ \mu\mathrm{m}$) with the DMI footprints plotted is illustrated in Fig. 2(b). Samples of the exact locations of MTB during the tracking phase are marked with triangles, and the respective estimated locations *via* DMI are marked with squares. Consider two swarms released simultaneously from the $1\mathrm{st}$ and the $4\mathrm{th}$ infusion sites. These two populations of MTB were guided by the magnetic fields to move for $2\ \mathrm{min}$ and reached the first aggregation zones where the tracking was performed. After tracking, the system was switched back to the propulsion-and-steering mode, where the agglomerations of MTB continued maneuvering and the DMI algorithm presented in [8] was applied to localize the MTB for the previous tracking cycle. This process was repeated periodically. When any of the two swarms left the breast, we released another agglomeration of MTB from the injection site next to it, and so on.

The general good agreement between the exact and estimated locations of the MTB demonstrates the efficacy of the DMI technique for tracking the CNTs-loaded bacteria microrobots. For well-planned swarm trajectories, a DMI footprint "sink" indicating the tumor location will be observed, as described in Section III. It is worth emphasizing that two additional MTB injections at the bottom of the breast phantom are introduced to complete the original survey plan pictured in Fig. 2(a).

Finally, we considered a typical multi-directional tumor targeting process based on the strategy presented in Section III (see also Fig. 1(d)). Fig. 2(c) demonstrates the final footsteps of MTB swarms for four tumors with varying sizes. As can be seen from this figure, the locations of these footprints correlate well with the size of the tumor, which demonstrates the potential of the proposed method for tumor size estimation.

V. Conclusion

This preliminary study presented novel strategies for microwave breast cancer detection and diagnosis with the use of multi-swarm bacterial microrobots. Several key assumptions must be verified for these tactics to be clinically feasible. These include the efficiency of the MTB as controlled trackable propulsion and steering systems, as well as the ability of our DMI algorithm to detect the MTB agglomerations based on the effect of their contrast agent cargos inside the tissue. Furthermore, the complex permittivity change due to the agent-attached swarms will depend on many factors and must be studied further.

Due to the physiological environment (microvasculature, tissue environment, etc.), it is more likely that the maximum density of MTB in the aggregation zone will be lower than the one achieved in free space such as in water. As such, the sensitivity of DMI for tracking MTB in the aggregation zone should be validated experimentally.

Finally, the immune response of MTB will be investigated further (e.g., development of mutation of the same specie of MTB for repeated operation within a short duration). Multimodality imaging including magnetic resonance imaging (MRI) will also be considered.

References

[1] N. K. Nikolova, "Microwave imaging for breast cancer," *IEEE Microw. Mag.*, vol. 12, no. 7, pp. 78-94, 2011.

[2] A. Mashal, B. Sitharaman, and *et al.*, "Toward carbon-nanotube-based theranostic agents for microwave detection and treatment of breast cancer: Enhanced dielectric and heating response of tissue-mimicking materials," *IEEE Trans. Biomed. Eng.*, vol. 57, pp. 1831-1834, Aug. 2010.

[3] G. Bellizzi, O. M. Bucci, and I. Catapano, "Microwave cancer imaging exploiting magnetic nanoparticles as contrast agent," *IEEE Trans. Biomed. Eng.*, vol. 58, no. 9, pp. 2528-2536, Sept. 2011.

[4] A. I. Minchinton and I. F. Tannock, "Drug penetration in solid tumours," *Nat. Rev. Cancer*, vol. 6, pp. 583-592, Aug. 2006.

[5] S. Martel, M. Mohammadi, and *et al.*, "Flagellated magnetotactic bacteria as contralled MRI-trackable propulsion and steering systems for medical nanorobots operating in the human microvasculature," *Int. J. Rob. Res.*, vol. 28, pp. 571-582, Apr. 2009.

[6] P. Kosmas and Y. Chen, "Possibilities for microwave breast tumor sensing via contrast-agent-loaded nanorobots," in *Proc. 2012 EuCAP*, Prague, Czech Republic, Mar. 2012.

[7] Y. Chen and P. Kosmas, "Detection and localization of tissue malignancy using contrast-enhanced microwave imaging: Exploring information theoretic criteria," *IEEE Trans. Biomed. Eng.*, vol. 59, pp. 766-776, Mar. 2012.

[8] Y. Chen and P. Kosmas, "Microwave breast tumor sensing and targeting using multiswarm contrast-agent-loaded bacterial nanorobots", in *Proc. ICEAA 2012*, Cape Town, South Africa, Sept. 2-7, 2012.

[9] E. Zastrow, S. K. Davis, and *et al.*, "Development of anatomically realistic numerical breast phantoms with accurate dielectric properties for modeling microwave interactions with the human breast," *IEEE Trans. Biomed. Eng.*, vol. 55, pp. 2792-2800, Dec. 2008.

[10] S. Martel, O. Felfoul, and *et al.*, "MRI-based medical nanorobotic platform for the control of magnetic nanoparticles and flagellated bacteria for target interventions in human capillaries," *Int. J. Rob. Res.*, vol. 28, pp. 1169-1182, Sept. 2009.